Impact of corrosion process of carbonyl iron particles on magnetorheological behavior of their suspensions

Tomas Plachy[1], Erika Kutalkova[1], Michal Sedlacik[1], Alenka Vesel[2], Milan Masar[1], Ivo Kuritka[1]

[1]*Centre of Polymer Systems, University Institute, Tomas Bata University in Zlín, Trida Tomase Bati 5678, 760 01 Zlín, Czech Republic*

[2]*Department of Surface Engineering and Optoelectronics, Jozef Stefan Institute, Jamova cesta 39, 1000 Ljubljana, Slovenia*

Abstract

The study investigates an influence of carbonyl iron (CI) particles' corrosion on magnetorheological performance of their silicone-oil suspensions. Carbonyl iron particles were oxidized thermally at 500 °C in the air or chemically in 0.05 HCl solution and the as-treated particles were subsequently used as a dispersed phase in magnetorheological suspensions. Corrosive layer on surface of oxidized particles was investigated using X-ray photoelectron spectroscopy (XPS) and X-ray diffraction (XRD). Obtained rheological data was treated with Robertson–Stiff (R-S) model to determine yield stress values and in order to find the yield stress values of prepared magnetorheological (MR) suspensions at saturation level a mathematical model was used. The suspensions based on oxidized particles showed lower values of the yield stress, which was significantly manifested at higher magnetic field intensities due to lower saturation magnetization of the particles.

Keywords

Carbonyl iron; thermal oxidation; magnetorheology; magnetorheological; magnetic particles; chemical oxidation

Introduction

Carbonyl iron is an iron-based powder material, which is widely used in an everyday life. One of the applications where CI is used due to its favorable magnetic properties are MR suspensions, which are systems whose rheological properties can be reversibly changed by a magnetic field [1-4]. They are generally composed of a non-magnetic liquid phase in which magnetic particles are randomly dispersed. Such suspensions behave as Newtonian or

pseudoplastic fluids; however, in the presence of an external magnetic field they start to act as viscoplastic solid due to creation of chain-like structures from magnetic particles along a direction of the applied magnetic field [5-8]. This transition and the stiffness of internal distribution of the particles within MR suspensions enables to control the viscosity of the systems, which is successfully utilized in many industrial applications [9-14].

From the long-term application point of view, the sedimentation [15] and chemical and thermo-oxidative stability of the MR suspensions are very challenging [16]. The CI particles are the main part of the MR devices and in long term period their ability to maintain their properties is of high importance. Carbonyl iron (generally iron) tends to undergo corrosion processes leading to oxidation of Fe to Fe^{2+} and Fe^{3+} [17] connected with formation of iron oxides in various forms (FeO, Fe_2O_3, Fe_3O_4) on its surface depending on the conditions. For example when iron is exposed to hydrochloric acid it forms ferrous chloride that further reacts to form solid Fe_2O_3. The oxidation of CI particles generally leads to a loose of their magnetic properties since iron oxides possess significantly lower saturation magnetization, M_S, than CI particles [4], and thus, this lowers the mechanical performance of MR devices. The failure of MR suspensions due to undergo oxidation process can be represented by few phenomena: (i) increase in field-off friction and leakage, (ii) decrease in MR effect due to lowering magnetic performance of particle, and (iii) increase in the field-off viscosity [18]. Ulicny et al. [19] investigated the durability of a MR clutch and it has been found that after 540 hours of durability test CI particles used in the MR clutch as a dispersed phase exhibited significant oxidation leading to lowering of torque capacity. An oxide layer was found on the surface of CI particles formed mainly by magnetite. It was further stated that the temperature in the gap area, in which the MR suspension is filled, can reach as high as 250 °C [19]. Moreover, oxidized particles can easily led to undesirable increase of field-off viscosity [20]. When the MR suspensions are exposed to high stresses, the brittle layer of iron oxides can be easily delaminated and thus significantly affect the rheology of MR suspensions [21, 22]. Abe et al. found that the level of oxidation of particles depends on the kind of the dispersive liquid and also found out the formation of a stabilized oxidation film on the surface of the particles. The change of the surface of the particles from the very smooth to very roughed was also observed [23]. Furthermore, a liquid medium in which the magnetic particles are suspended can undergo a decrease in molecular weight in a long-term service [24].

There are efforts to protect CI particles from oxidation using polymeric shell coatings [25-28], silica coating of CI particles increasing their thermal and chemical oxidation stability [29, 30],

and recently inorganic films based on rare earth elements were successfully introduced on surface of CI particles providing increased chemical and thermal oxidation [31]. However, the impact of oxidation of CI particles on their MR performance has not been quantitatively evaluated yet. The polymeric or inorganic shell on their surface enhances thermal as well as chemical stability of CI particles, nevertheless, the oxidation is not fully inhibited and the coating process also significantly increases the price of MR devices.

This study deals with an impact of thermal and chemical oxidative processes of CI particles on MR performance of their silicone-oil suspensions. Two batches of oxidized CI particles were prepared, the first one through a thermal treatment at 500 °C in the air and the second one by chemical oxidation of CI particles in 0.05 M HCl solution. The oxidation of the particles was evaluated using XPS, XRD and scanning electron microscopy (SEM). A silicone-oil suspension based on non-oxidized CI particles was used as a reference MR suspension.

Experimental part

Sample preparation

Pure CI particles (grade ES; BASF, Germany) were used as a precursor and also as a reference material. The CI particles were further thermally or chemically oxidized, thus, two new samples were prepared using extreme conditions in order to evaluate a high level of the oxidation.

Thermal oxidation

Pure CI particles were treated in a furnace at 500 °C in the air. They were put to the furnace in a ceramic mortar at a room temperature and the heating rate was 10 °C/min. After reaching the final temperature, the furnace was switched off and the particles were left to cool down to room temperature. The gain weight of the particles through thermal oxidation process was about 30.6 % due to formation of iron oxides, which fits well with the study presented by Mrlik et al. [16]. These particles are further labelled as CI ES–500.

Chemical oxidation

Pure CI particles were treated in a solution of 0.05 M HCl. This concentration was taken according to the literature, where 0.05 M HCl is often used for the investigation of the chemical stability of modified CI particles with a polymeric shell [25, 26, 32]. Briefly, CI particles were

immersed in 0.05 M HCl overnight and the system was gently mixed using an external mixer. The acidic solution was then left to evaporate at 60 °C and the particles were further dried at 70 °C in a vacuum oven for 24 hours. The gain weight of the particles through chemical oxidation was 9.0 %. The particles are further labeled as CI ES-HCl.

Particles characterization: XRD, XPS, SEM, magnetization measurements

The crystalline phase structures of prepared materials were identified using X-ray diffractometer MiniFlex 600 (RIGAKU, Japan) equipped with Co X-ray source. Operation voltage and current being 40 kV and 15 mA, respectively. X-ray photoelectron spectroscopy measurements were performed using a TFA XPS device from Physical Electronics. The base pressure in the XPS analysis chamber was approximately 6×10^{-8} Pa. The samples were excited by X-rays over a 400 μm^2 spot area with monochromatic Al $K\alpha_{1,2}$ radiation at 1486.6 eV. Photoelectrons were detected with a hemispherical analyser positioned at an angle of 45° with respect to the normal to the sample surface. Survey-scan spectra were acquired at a pass energy of 187.85 eV and with 0.4 eV energy step, whereas for Fe 2p, individual high-resolution spectra were taken at a pass energy of 58 eV and with a 0.125 eV energy step. All the spectra were referenced to the main C 1s peak of the carbon atoms, which was assigned a value of 284.8 eV. The spectra were analysed using MultiPak v8.1c software (Ulvac-Phi Inc., Kanagawa, Japan, 2006) from Physical Electronics, which was supplied with the spectrometer. Morphology and size of the particles were investigated using SEM analysis (FEI, NanoSEM450, USA). Magnetization curves of particles were measured by a vibrational sample magnetometer (VSM; Model 7404, Lake Shore, USA) in the magnetic field range of ±760 kA m^{-1} at a room temperature.

Preparation of MR suspensions

Three MR suspensions were prepared by mixing of the prepared samples with silicone oil (Lukosiol M200, Chemical Works Kolín, Czech Republic, viscosity η_c = 194 mPa s). The concentration of the particles in the prepared MR suspensions was always adapted to contain 40 wt% of pure CI. Thus, in the case of MR suspensions based on CI ES, the concentration of the particles was 40 wt%, in the case of MR suspensions based on CI ES–500 or CI ES-HCl the concentration of the particles was 40 wt% of the pure CI + oxidized mass.

Magnetorheological measurements

Rheological measurements of the prepared MR suspensions were performed at the shear rates 0.01-100 s^{-1} using a rotational rheometer (MCR 502 Anton Paar, Austria) with an external magnetic cell and a plate-plate geometry with a gap of 300 μm. The MR measurements were carried out in the presence of an external magnetic field of intensity, *H*, 173–438 kA/m. Before each measurement, the prepared MR suspensions were intensively mixed for about 5 min and in the case of measurement in the presence of an external magnetic field, the magnetic field was applied for 1 min before the measurement in order to provide time enough for the particles to create stable chain-like structures. The measurements were carried out 3 times with a fresh sample for each MR suspension.

Results and discussion

Particle characterization

Tab. 1 shows the surface composition of the samples as deduced from the survey-scan spectra shown in Fig. 1. The surfaces of samples are composed of carbon, oxygen and iron, whereas for sample CI ES–HCl also some chlorine was found on the surface (Tab. 1). The chlorine is clearly residual amount from the oxidation process.

Tab. 1. Surface composition (in atomic %) of the samples as determined from XPS survey spectra (average of two measurements).

Chemical element	CI ES	CI ES–500	CI ES–HCl
C	45.4	25.2	28.0
O	42.2	59.0	56.0
Fe	12.4	15.8	15.9
Cl	–	–	3.3
O/Fe	3.39	3.73	3.48

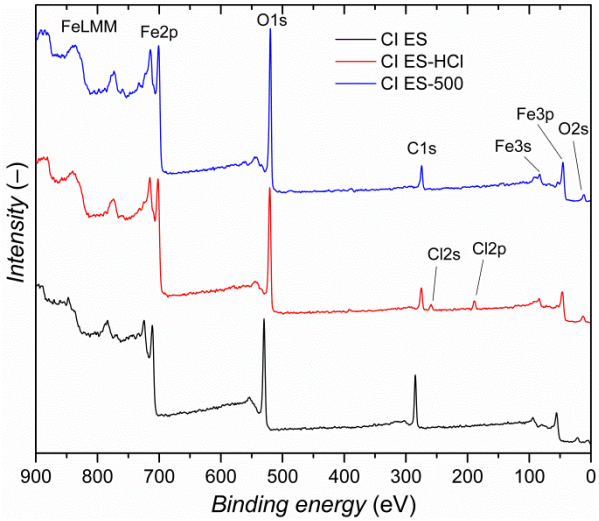

Fig. 1. XPS survey spectra of the samples (top spectrum) CI ES-500, (middle spectrum) CI ES-HCl, and (bottom spectrum) CI ES.

Fig. 2 depicts comparison of high-resolution Fe2p peaks for all three samples. Fe2p peak consists of doublet peaks $Fe2p_{3/2}$ and $Fe2p_{1/2}$. There is also a clearly distinguishable additional satellite peak. It can be observed that the peak position, the shape, and the width of the peaks are similar for all samples. The position of $Fe2p_{3/2}$ and $Fe2p_{1/2}$ peaks is approximately 710.9 and 724.5 eV, respectively. This binding energy is typical for Fe^{3+} ions in Fe_2O_3 oxides [33, 34]. The satellite peak is positioned at approximately 719.1 eV, which is about 8.2 eV higher than the position of the main $Fe2p_{3/2}$ peak. As reported in the literature, this binding energy of the satellite peak is characteristic for Fe_2O_3 oxide [33]. The satellite peak is often used for interpretation of iron oxides, because its position is very sensitive to the oxidation state of iron [33]. For example, it was reported that a satellite peak for FeO (Fe^{2+} ions) appears at a lower binding energy of approximately 715.5 eV, whereas for Fe_3O_4 the satellite peak is not observed [33, 34]. Also the main $2p_{3/2}$ peak for FeO and Fe_3O_4 should appear at a lower binding energy than in the case of Fe_2O_3 [33] which would result in formation of a shoulder on the measured $Fe2p_{3/2}$ curve on the low-energy side. The $2p_{3/2}$ peak for FeO and Fe_3O_4 should be at approximately 708-709 eV and ~710 eV, respectively [33-36]. In Fig. 2a it can be clearly observed that there is no such shoulder. Because of the lack of the satellite at 715.5 eV and a shoulder at ~708-709 eV, we can explicitly exclude formation of FeO, whereas any presence of Fe_3O_4 is still doubtful. According to Yamashita, Fe_3O_4 could be (because of its stoichiometric nature) expressed also as $FeO{\cdot}Fe_2O_3$ with the ratio of Fe^{2+}/Fe^{3+} ions equal to 1:2 [33]. However, any attempt to make deconvolution of the peaks in Fig. 2a to Fe^{3+} and Fe^{2+} states was impossible. Therefore, the Fe3p peak was also measured, because it was reported that this peak can be used for obtaining information on concentrations of Fe^{2+} and Fe^{3+} ions [33, 36]. Again, there is now difference between the spectra (Fig. 2b). The spectra are similar to spectrum of Fe_2O_3 standard published by Yamashita [33] and there is no indication of appearance of a shoulder at lower binding energies which would indicate the presence of Fe^{2+} ions. Therefore, it can be concluded that the surfaces of all three samples are composed primary of Fe_2O_3 oxide.

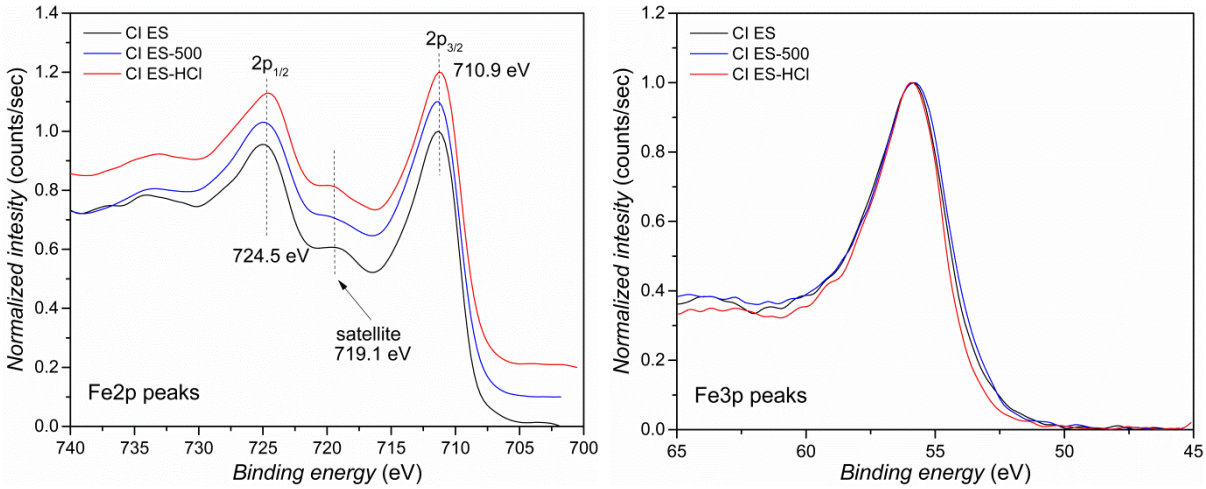

Fig. 2. Comparison of high-resolution XPS spectra for (left figure) iron Fe2p peaks and for (right figure) Fe3p peaks for all three samples.

It should be noted, that all samples were exposed to air during handling and storage and even if there is any Fe_3O_4 phase (actually magnetite) present in the sample, the few surface atomic layers will be always fully oxidized to maghemite (Fe_2O_3) due to air and omnipresent moisture. Moreover, the strong signal of carbon (C1s peak in the spectrum in Fig. 1) testifies for presence of adventitious carbon, which origins most likely from unavoidable contamination of air-exposed samples as well as from eventual organic solvent treatment steps during sample manipulation.

X-ray diffractograms of CI ES and its forms oxidized at 500 °C or in 0.05 M HCl are shown in Fig 3. Pure CI ES diffraction peaks were indexed to the standard data of the iron (PDF Card No.: 01-080-3816) with the characteristic peak at 52.32° (110). In both oxidized samples a peak at 52.37° (110) reflecting pure iron was also found, even though its intensity in the case of the sample CI ES–500 significantly decreased due to strong oxidation. X-ray diffractograms of CI ES–500 and CI ES–HCl were further compared to the standard data of magnetite (PDF Card No.: 01-087-2334) and maghemite (PDF Card No.: 01-089-5892). Both samples exhibit peaks characteristic for either maghemite (Fe_2O_3) or magnetite (Fe_3O_4) while the spectrum of CI ES–500 differs more significantly from that one for pure CI ES indicating stronger oxidation and higher intensity of peaks representing maghemite phase occurs. Presence of both phases fits well with literature when an exhibition of steel at temperatures 400–550 °C in the presence of supercritical water led to formation of both phases [37]. Using XRD it is very challenging to credibly distinguish between these two phases, nevertheless, it can be concluded that the

thermal and chemical oxidation of CI particles lead to formation of various iron oxides on its surface which further results in a change of their properties. When compared to the XPS technique, XPS examines only few nanometres (≈ 2 nm) of the surface [38], where only Fe_2O_3 is presented. Indeed, Fe_3O_4 converts into Fe_2O_3 on the air [39] which can elucidate eventual difference in findings from XPS and XRD measurements. Moreover, annealing of magnetite at high temperature (hundreds °C) in air atmosphere leads to the oxidation of all Fe^{2+} ions causing transition of eventual magnetite phase to maghemite.

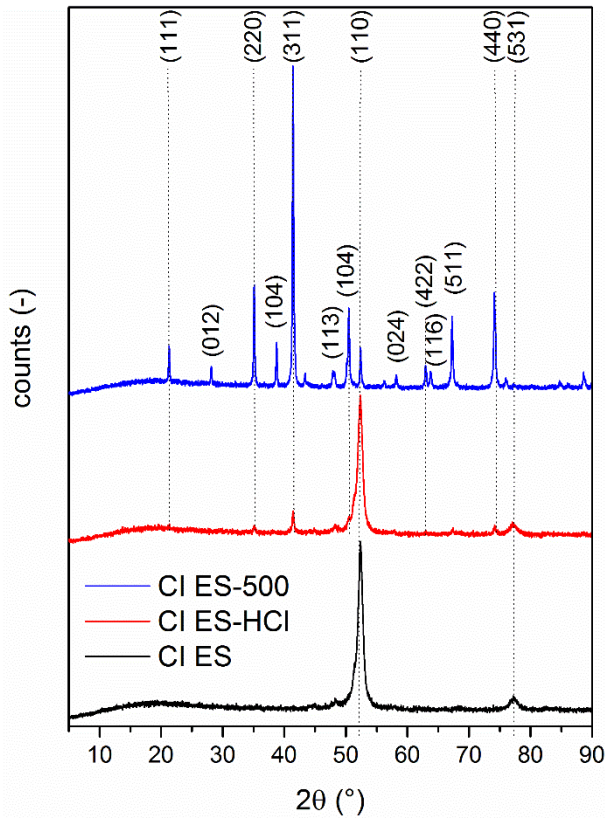

Fig. 3. XRD patterns of CI ES–500, CI ES–HCl, and CI ES particles.

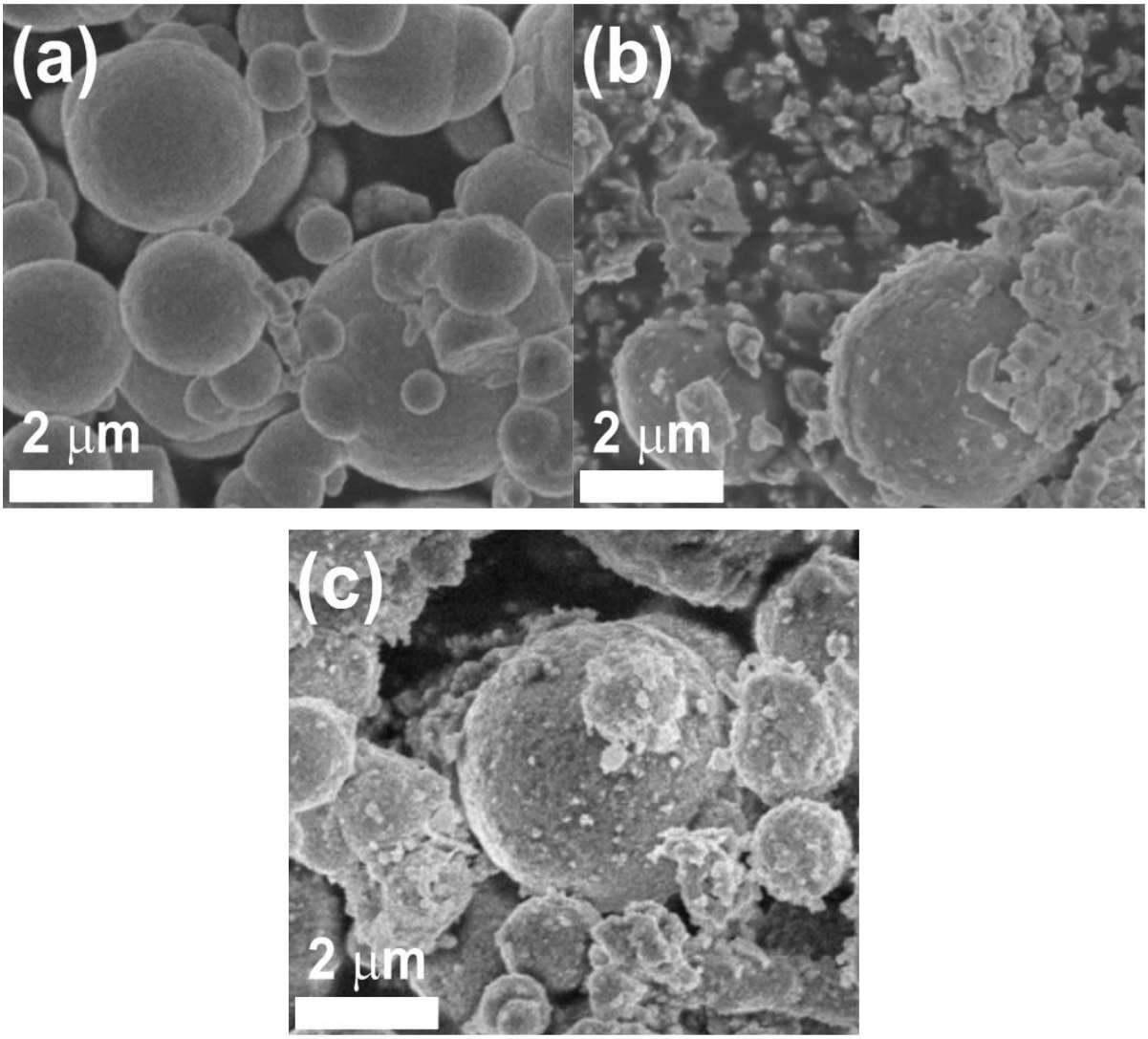

Fig. 4. SEM images of (a) CI ES, (b) CI ES–500, and (c) CI ES–HCl.

Pure CI ES consists of few micron-sized particles possessing a spherical shape with a smooth surface and relatively high polydispersity (Fig. 4a). The both corroded particles sustain their spherical shape, however, the oxidation process caused formation of smaller adherent particles or flakes from highly oxidized parts of original CI particles. This phenomenon is evident in the case of the sample CI ES-500 (Fig. 4b). While in the case of CI ES–500 the formation of smaller irregular particles is evident (Fig. 4b), in the case of CI ES–HCl (Fig. 4c) only the roughness of the particles surface clearly increased. The creation of smaller particles in thermally oxidized sample can be elucidated by peeling process of oxide flakes or smaller particles that can take part in the case of iron oxides at 500 °C due to large difference in elemental cell size of iron and iron oxides. Thus, the elevated temperature leads to oxidation of the CIs and the rose up iron oxides can fragment or even create aggregate further sintering together and create microscopic particles standing alone not bound to the original CI particles.

Oxidation process further significantly affects magnetization properties of the particles; their magnetization curves are depicted in Fig. 5. The highest saturation magnetization, M_S, was observed first things first for the samples CI ES > CI ES–HCl > CI ES–500 with the values of M_S 186.6, 149.9, and 68.8 emu g^{-1}, respectively. While the CI ES particles are composed nearly only from pure iron, with a very thin oxidized layer, the oxidation process at higher temperatures or in an acid source led to formation of maghemite (Fe_2O_3), with significantly lower M_S than the pure CI [4, 40, 41]. Moreover, oxides are formed at the expense of iron which lowers content of the component with high M_S. Therefore, the oxidized samples possess significantly lower M_S. Let us assume that the composition of oxide layer is approximately Fe_2O_3 while the core is purely from Fe. On the base of simple chemical balance according to theoretical calculations regarding the change in volume of particles (obtained from tabular densities) connected with oxidation of pure iron to Fe_2O_3, the calculated M_S values for CI ES, CI ES–HCl, CI ES–500 were 186.6, 146.2, and 72.0 emu g^{-1}, respectively, which fits well the measured values. As reference M_S values were used 186.6 emu g^{-1} for CI ES (experimentally verified value) and 40 emu g^{-1} for Fe_2O_3 (40 emu g^{-1} as the best guess that corresponds to the mean M_S value of the mixture of non-magnetic hematite together with maghemite [42]). Weight percentage of components was used as the base for simple linear mixing rule for calculation of M_S. It was noticed also, that oxidation process slightly increased remanent magnetization.

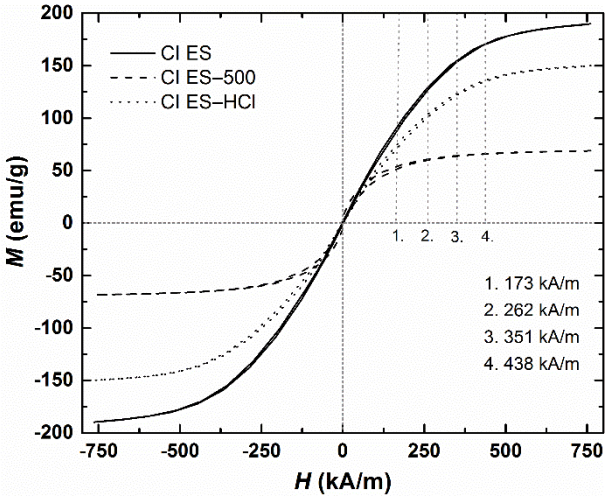

Fig. 5. Magnetization curves for CI ES, CI ES-500, and CI ES-HCl particles. The values 1.-4. represent the magnetic field intensities used during MR measurements.

Magnetorheological measurements

The oxidized particles where further used as a dispersed phase in MR suspensions and their behavior was compared with the pure CI ES silicone-oil suspensions. While in the absence of an external magnetic field prepared MR suspensions behave as pseudoplastic fluids, upon an application of magnetic field they start to act as a viscoplastic fluid exhibiting a yield stress, τ_y (Fig. 6). The highest transition to a viscoplastic fluid is observed for the MR suspension based on bare CI ES particles due to their magnetic properties (Fig. 5), and the MR suspension based on CI ES–HCl particles exhibit higher values of shear stress than MR suspension based on CI ES–500 particles. Further, with increasing magnetic field intensity the difference in rheological parameters between the prepared suspensions increases. This is a consequence of magnetic properties of the particles, where at low magnetic field intensities (≦ 173 kA/m) their magnetizations are similar (Fig. 5). With further increase in magnetic field intensity, however, the high difference between magnetization of the particles occurs leading to the significant differences in MR behavior of their suspensions.

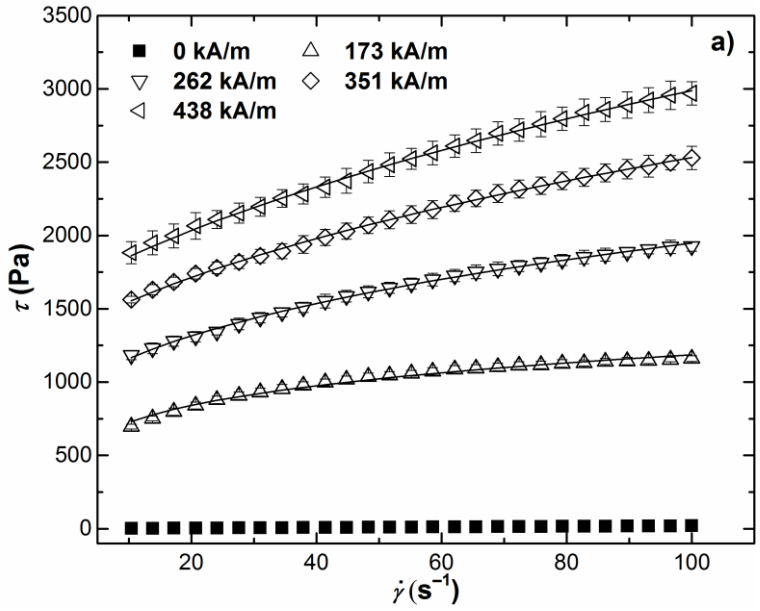

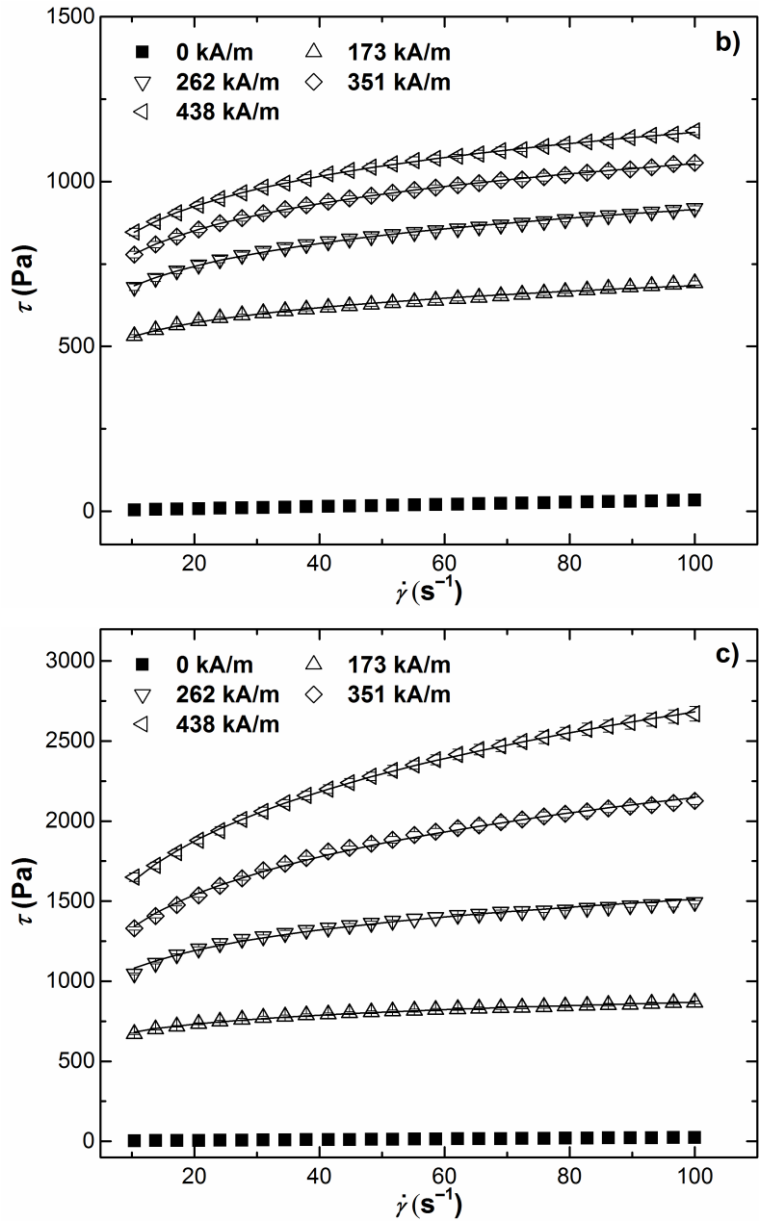

Fig. 6. The dependence of τ vs. $\dot{\gamma}$ for MR suspensions based on (a) CI ES, (b) CI ES–500, and (c) CI ES–HCl particles at various magnetic field intensities.

One of the important parameters of the MR suspensions is the value of the τ_y, representing the stress that the suspensions can withstand before they start to flow [15, 43]. The Robertson–Stiff (R–S) model (Eq. 1), which has been recently successfully used for modeling of flow curves for MR suspensions [44], was implemented to obtain τ_y values and thus to quantify the impact of corrosion of the CI particles on MR performance of their silicone-oil suspensions. In R–S model *K* and *n* represent consistency and flow behavior index [44], respectively.

$$\tau = \left[K^{\frac{1}{n}} |\dot{\gamma}|^{\frac{n-1}{1}} + \left(\frac{\tau_y}{|\dot{\gamma}|}\right)^{\frac{1}{n}} \right]^n \dot{\gamma} \quad (1)$$

These values of τ_y increase with the magnetic field intensity (Tab. 2). The highest values of τ_y exhibited the MR suspensions based on pure CI ES due to their most favorable magnetic properties. The influence of CI particles oxidation on their MR behavior possess high impact mainly at higher magnetic field intensities (>173 kA/m) due to significant decrease in M_S of oxidized particles (Fig. 5). While in the lower magnetic fields τ_y depends mainly on magnetic field intensity and scales as $\tau_y \sim H^2$ at the higher magnetic fields M_S value starts to be important and τ_y further scales as $\tau_y \sim M_S^{1/2} H^{3/2}$ [45, 46]. Since the difference in magnetization of the particles increases with increasing magnetic field intensity, the higher magnetic field intensity the higher difference in τ_y of the prepared MR suspensions. Magnetorheological suspensions based on the thermally-treated particles show the lowest τ_y values. The abrupt increase of parameter K can be explained as an increase of inherent viscosity of the systems after application of magnetic field, and on the other side, the decrease of parameter n can be attributed to change in flow behavior in the presence of magnetic field.

Tab. 2. Values of τ_y (in Pa), parameters K (Pa s^n) and n (-) obtained with applying of R–S model on the flow curves of prepared MR suspensions at various magnetic field intensities.

MR suspension	Magnetic field intensity (kA/m)	Parameter τ_y (Pa)	Parameter K (Pa s^n)	Parameter n (-)
CI ES	0	0.38 ± 0.04	0.21 ± 0.00	0.97 ± 0.01
	173	432 ± 8	401 ± 4	0.23 ± 0.01
	262	906 ± 19	435 ± 17	0.31 ± 0.01
	351	1320 ± 20	432 ± 21	0.37 ± 0.02
	438	1630 ± 80	449 ± 24	0.39 ± 0.01
CI ES–HCl	0	0.59 ± 0.17	0.26 ± 0.05	0.97 ± 0.02
	173	390 ± 10	528 ± 9	0.11 ± 0.01
	262	623 ± 8	773 ± 28	0.14 ± 0.01
	351	950 ± 18	818 ± 47	0.21 ± 0.02
	438	1210 ± 40	948 ± 51	0.22 ± 0.01
CI ES–500	0	0.52 ± 0.12	0.47 ± 0.01	0.93 ± 0.01
	173	285 ± 4	406 ± 16	0.11 ± 0.01
	262	440 ± 30	500 ± 17	0.13 ± 0.00

	351	576 ± 14	572 ± 32	0.13 ± 0.01
	438	645 ± 18	616 ± 26	0.14 ± 0.01

It was found that the level of oxidation significantly affects the saturation characteristic of the oxidized CI particles and thus also the τ_y values. Due to the utilized technical device, performed MR measurements were conducted below M_S of the particles and in order to find τ_y of prepared MR suspensions at saturation level of the particles a mathematical model was used. It is well known that at high magnetic fields close saturation magnetization of the particles τ_y scales as $\tau_y \sim M_S^2$ [47] and Varela-Jiménez et al. [48] have further proposed a constitutive model for the prediction of the τ_y values as a function of an applied magnetic field (Eq. 2).

$$\tau_y = \left[1 + \left(\frac{H}{H_C}\right)^{-B_{MRF}}\right]^{-1} \cdot \left[\frac{4}{5^{2.5}} \cdot \varepsilon(3) \cdot \varphi \cdot \mu_0 \cdot M_S^2\right] \qquad (2)$$

In Eq. 2 B_{MRF} is a constant for each specific system [48], μ_0 represents magnetic constant (vacuum permeability), φ is a particle volume fraction, H_c is the characteristic magnetic field at which 50 % of the state transition occurs, and $\varepsilon(3)$ is equal to 1.202 [46]. The left term in this equation represents a sigmoidal curve describing the shape of the dependence of τ_y on the applied magnetic field intensity while term on the right side is actually a constant representing the maximum value of τ_y reached at the magnetic field intensity sufficient to achieve complete magnetic saturation of all particles. With the use of the right term, it was calculated that τ_y values at M_S of investigated particles are 25.5 kPa, 15.3 kPa, and 4.0 kPa for CI ES, CI ES–HCl, and CI ES–500, respectively. Then, the dependencies described by Eq. 2 were fitted into experimental data. The result of this procedure is plotted in the graph in Fig. 7.

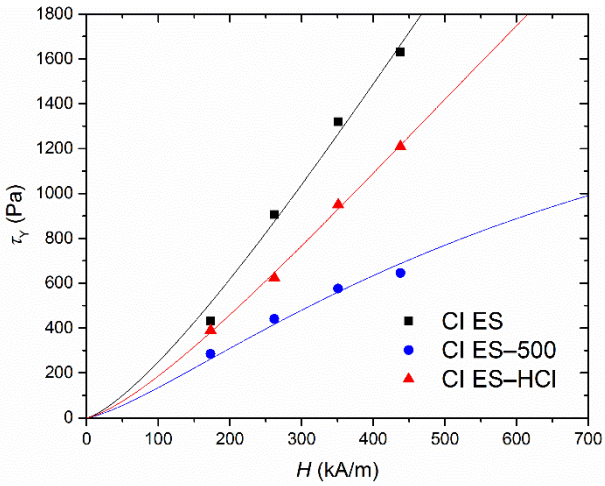

Fig. 7. The dependence of τ_Y on the *H* for the prepared MR suspensions based on CI ES, CI ES–500, and CI ES–HCl particles at various magnetic field intensities. The solid lines represent fits according to constitutive model presented in Ref. [48] (eq. 2).

From the application point of view the behavior under dynamic loading is of high interest. The cyclic loading of the materials represent the possibility to repeatedly load the systems under they would undergo a failure. Fig. 8 represents storage modulus, *G´*, and loss modulus, *G´´*, dependence on the frequency, *f*, in a linear viscoelastic region of the systems. The significantly higher values of *G´* over *G´´* reflects the rigidity of the system in a presence of a magnetic field confirming transition from liquid-like system to a viscoplastic solid. It can be further seen that the MR suspensions based on non-oxidized particles exhibit the highest MR performance proving the importance of preventing the particles from the oxidation when used in MR suspensions.

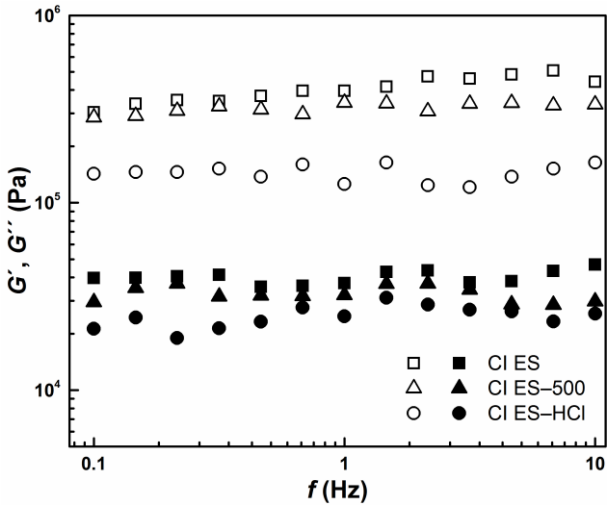

Fig. 8. The dependence of elastic, *G´*, and loss modulus, *G´´*, on the frequency, *f*, for prepared MR suspensions in the presence of an external magnetic field of intensity 438 kA/m.

Conclusions

The effect of oxidation of carbonyl iron particles on magnetorheological behavior of their silicone-oil suspension was investigated. Carbonyl iron particles were oxidized at two levels: (i) by a fierce thermal oxidation at 500 °C in the air and (ii) by a mild chemical oxidation in 0.05 M HCl. Pure non-oxidized carbonyl iron particles were used as a reference. X-ray photoelectron spectroscopy and X-ray diffraction were used to investigate the changes of the particles arisen from the oxidative processes. In both cases the presence of various forms of iron oxides was confirmed leading to significant decrease in the magnetization saturation of the

particles. The oxidized particles were further used as a dispersed phase in magnetorheological suspensions. Both magnetorheological suspensions exhibited lower rheological parameters than the system based on original carbonyl iron particles due to lower magnetic saturation of the oxidized ones, whereas the thermally-oxidized particles possessed the lowest yield stress more than two times lower than the suspension based on the original particles, which was quantitatively evaluated using Robertson–Stiff model. It was predicted that at saturation level the yield stress of the oxidized particles decreases about 5 times when compared to non-oxidized particles.

Author contributions

The manuscript was written through contributions of all authors. All authors have given approval to the final version of the manuscript.

Acknowledgment

This work was supported by the Ministry of Education, Youth and Sports of the Czech Republic – Program NPU I (LO1504). This research was also carried out with support of the Operational Program Research and Development for Innovations co-funded by the European Regional Development Fund (ERDF) and national budget of the Czech Republic, within the framework of the Centre of Polymer Systems project (CZ.1.05/2.1.00/19.0409).

Data availability

Data will be made available on request.

References

[1] M.T. Lopez-Lopez, J. de Vicente, F. Gonzalez-Caballero, J.D.G. Duran, Colloid Surf. A-Physicochem. Eng. Asp., 264 (2005) 75-81.
[2] M. Machovsky, M. Mrlik, T. Plachy, I. Kuritka, V. Pavlinek, Z. Kozakova, T. Kitano, RSC Adv., 5 (2015) 19213-19219.
[3] M. Mrlik, M. Ilcikova, M. Cvek, V. Pavlinek, A. Zahoranova, Z. Kronekova, P. Kasak, RSC Adv., 6 (2016) 32823-32830.
[4] T. Plachy, M. Cvek, Z. Kozakova, M. Sedlacik, R. Moucka, Smart Materials and Structures, 26 (2017).
[5] R.C. Bell, J.O. Karli, A.N. Vavreck, D.T. Zimmerman, G.T. Ngatu, N.M. Wereley, Smart Mater. Struct., 17 (2008) 6.
[6] M. Cvek, M. Mrlik, M. Ilcikova, T. Plachy, M. Sedlacik, J. Mosnacek, V. Pavlinek, J. Mater. Chem. C, 3 (2015) 4646-4656.

[7] J. de Vicente, D.J. Klingenberg, R. Hidalgo-Alvarez, Soft Matter, 7 (2011) 3701-3710.
[8] L. Rodriguez-Arco, M.T. Lopez-Lopez, P. Kuzhir, F. Gonzalez-Caballero, Phys. Rev. E, 90 (2014) 11.
[9] M. Bitaraf, O.E. Ozbulut, S. Hurlebaus, L. Barroso, Eng. Struct., 32 (2010) 3040-3047.
[10] F. Bucchi, P. Forte, A. Franceschini, F. Frendo, Smart Materials and Structures, 22 (2013) 10.
[11] Z.Q. Chen, X.Y. Wang, J.M. Ko, Y.Q. Ni, B.F. Spencer, G. Yang, in MR damping system on Dongting Lake cable-stayed bridge, S.C. Liu Ed., pp. 229-235, Spie-Int Soc Optical Engineering, Bellingham (2003).
[12] Z.Q. Chen, X.Y. Wang, J.M. Ko, Y.Q. Ni, B.F. Spencer, G. Yang, J.H. Hu, Wind Struct., 7 (2004) 293-304.
[13] S. Nagai, H. Tomori, Y. Midorikawa, T. Nakamura, Ieee, in The position and vibration control of the artificial muscle manipulator by variable viscosity coefficient using MR brake, Ieee, New York (2011).
[14] X.C. Zhu, X.J. Jing, L. Cheng, J. Intell. Mater. Syst. Struct., 23 (2012) 839-873.
[15] G.S. Wang, Y.Y. Ma, Y. Tong, X.F. Dong, J. Ind. Eng. Chem., 48 (2017) 142-150.
[16] M. Mrlik, M. Ilcikova, V. Pavlinek, J. Mosnacek, P. Peer, P. Filip, J. Colloid Interface Sci., 396 (2013) 146-151.
[17] M.W. Tan, E. Akiyama, A. Kawashima, K. Asami, K. Hashimoto, Corrosion Sci., 37 (1995) 331-341.
[18] A. Wiehe, J. Maas, J. Intell. Mater. Syst. Struct., 24 (2013) 1433-1444.
[19] J.C. Ulicny, M.P. Balogh, N.M. Potter, R.A. Waldo, Mater. Sci. Eng. A-Struct. Mater. Prop. Microstruct. Process., 443 (2007) 16-24.
[20] J. Roupec, I. Mazurek, Stability of Magnetorheological Effect during Long Term Operation, Springer-Verlag Berlin, Berlin (2011).
[21] J.D. Carlson, J. Intell. Mater. Syst. Struct., 13 (2002) 431-435.
[22] J. Roupec, I. Mazurek, Z. Strecker, M. Klapka, in The behavior of the MR fluid during durability test, H.I. Unal Ed., Iop Publishing Ltd, Bristol (2013).
[23] I. Abe, T. Kikuchi, J. Noma, Smart Materials and Structures, 26 (2017) 11.
[24] J.C. Ulicny, C.A. Hayden, P.A. Hanley, D.F. Eckel, Mater. Sci. Eng. A-Struct. Mater. Prop. Microstruct. Process., 464 (2007) 269-273.
[25] M. Cvek, M. Mrlik, M. Ilcikova, J. Mosnacek, V. Babayan, Z. Kucekova, P. Humpolicek, V. Pavlinek, RSC Adv., 5 (2015) 72816-72824.
[26] M. Sedlacik, V. Pavlinek, R. Vyroubal, P. Peer, P. Filip, Smart Materials and Structures, 22 (2013) 8.
[27] T. Shimura, K. Aramaki, Corrosion Sci., 50 (2008) 2407-2414.
[28] M. Sedlacik, V. Pavlinek, RSC Adv., 4 (2014) 58377-58385.
[29] Y.D. Liu, F.F. Fang, H.J. Choi, Colloid Polym. Sci., 289 (2011) 1295-1298.
[30] Y.D. Liu, H.J. Choi, S.B. Choi, Colloid Surf. A-Physicochem. Eng. Asp., 403 (2012) 133-138.
[31] A. Esmaeilzare, S.M. Rezaei, B. Ramezanzadeh, Appl. Surf. Sci., 436 (2018) 1200-1212.
[32] M. Mrlik, V. Pavlinek, Smart Materials and Structures, 25 (2016) 10.
[33] T. Yamashita, P. Hayes, Applied Surface Science, 254 (2008) 2441-2449.
[34] C.S. Doyle, C.K. Seal, B.J. James, Applied Surface Science, 257 (2011) 10005-10017.
[35] T. Fujii, F.M.F. de Groot, G.A. Sawatzky, F.C. Voogt, T. Hibma, K. Okada, Phys Rev B, 59 (1999) 3195-3202.
[36] S. Gyergyek, D. Makovec, M. Jagodič, M. Drofenik, K. Schenk, O. Jordan, J. Kovač, G. Dražič, H. Hofmann, Journal of Alloys and Compounds, 694 (2017) 261-271.
[37] X.Y. Zhong, X.Q. Wu, E.H. Han, Corrosion Sci., 90 (2015) 511-521.

[38] N.I.o.S.a. Technology, in NIST Electron inelastic-Mean-Free-Path Database, U.S.Department of Commerce, Maryland, USA (2000).
[39] B.E. Monsen, S.E. Olsen, L. Kolbeinsen, Scand. J. Metall., 23 (1994) 74-80.
[40] A. Millan, F. Palacio, A. Falqui, E. Snoeck, V. Serin, A. Bhattacharjee, V. Ksenofontov, P. Gutlich, I. Gilbert, Acta Mater., 55 (2007) 2201-2209.
[41] H. Gavilan, O. Posth, L.K. Bogart, U. Steinhoff, L. Gutierrez, M.P. Morales, Acta Mater., 125 (2017) 416-424.
[42] A.S. Teja, P.Y. Koh, Prog. Cryst. Growth Charact. Mater., 55 (2009) 22-45.
[43] H.S. Chae, S.H. Piao, H.J. Choi, J. Ind. Eng. Chem., 29 (2015) 129-133.
[44] M. Cvek, M. Mrlik, V. Pavlinek, J. Rheol., 60 (2016) 687.
[45] F.F. Fang, Y.D. Liu, H.J. Choi, Y. Seo, ACS Appl. Mater. Interfaces, 3 (2011) 3487-3495.
[46] J.M. Ginder, L.C. Davis, L.D. Elie, Int. J. Mod. Phys. B, 10 (1996) 3293-3303.
[47] J.M. Ginder, L.C. Davis, Appl. Phys. Lett., 65 (1994) 3410-3412.
[48] M.I. Varela-Jimenez, J.L.V. Luna, J.A. Cortes-Ramirez, G. Song, Smart Materials and Structures, 24 (2015) 7.